Time-Resolved EPR Studies of Main Chain Radicals from Acrylic Polymers. Structural Characterization at High Temperatures

Vanessa P. McCaffrey and Malcolm D. E. Forbes*

Venable and Kenan Laboratories, Department of Chemistry, CB #3290, University of North Carolina, Chapel Hill, North Carolina 27599

Received October 17, 2004; Revised Manuscript Received January 7, 2005

ABSTRACT: Main chain radicals from several acrylic polymers are characterized in liquid solution at high temperatures (∼100 °C) using time-resolved electron paramagnetic resonance (TREPR) spectroscopy. The radicals are produced by laser flash photolysis (248 nm) and subsequent loss of the side chain ester functionality by Norrish I α-cleavage. At these temperatures fast-motion spectra with conformationally averaged hyperfine interactions are observed. The spectra are strongly spin polarized from the triplet mechanism (TM) of chemically induced dynamic electron spin polarization (CIDEP). Computer simulation of the TREPR spectra leads to unambiguous structural characterization of both the main chain radical and the side chain oxo-acyl radical. Hyperfine coupling constants, *g*-factors, and line widths are reported and discussed for radicals produced from five different acrylic polymers. Variation of the side chain on the polymer backbone leads to significant changes in the observed hyperfine coupling constants. For the main chain radical from poly(fluorooctyl methacrylate) (PFOMA), fast motion of the polymer chain is not accessible at these temperatures. The side chain oxo-acyl radical from PFOMA exhibits long-range ^{19}F hyperfine interactions. Additional TREPR experiments on small molecule model compounds and gel permeation chromotography results of the photolyzed polymers support the conclusion that the primary photodegradation mechanism proposed in this paper is general for acrylic polymers.

Introduction

Photodegradation of polymers is a subject of intense interest, particularly in the areas of lithographic photoresists and the weathering of architectural coatings. The successful development of more robust coatings and the controlled degradation of photoresists both rely on a detailed understanding of the degradation mechanism. In 2000, we reported the first structural characterization of main chain polymeric free radicals formed by UV photolysis of acrylic polymers in liquid solution using time-resolved electron paramagnetic resonance spectroscopy (TREPR).[1] The focus of our previous paper was on the symmetry properties of these free radicals as a function of polymer tacticity under fast-motion (high-temperature) conditions for poly(methyl methacrylate) (PMMA) and poly(ethyl acrylate) (PEA), structures **1** and **2** in Chart 1, respectively.

We have recently expanded the scope of this research to the study of several additional acrylic polymers and related structures, also shown in Chart 1. Structural modification of acrylates can be achieved at two sites which are important to distinguish. The first modification is that of the substituent of the polymer backbone, and the second is that of the ester side chain. We will refer to these modifications using the more common polymer nomenclature for main chain and side chain sites as α substitution and *β* substitution, respectively. The most structurally simple acrylic polymer we have studied is poly(ethyl acrylate), PEA (**2**), which has hydrogen as the α-substituent. Of the remaining five acrylic polymers we have studied, four are methacrylates (**1**, **3**−**5**). The last of these methacrylates is poly(fluorooctyl methacrylate) (PFOMA, **5**), which has very different physical properties than the first four methacrylates due to the bulky (and more rigid) *β*-substituent (see discussion below for more details on PFOMA). The remaining acrylic polymer in Chart 1 is poly(ethyl cyanoacrylate) (PECA, **6**) where the α-substituent is a nitrile group.

Chart 1

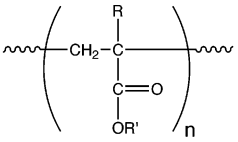

	Polymer	Acronym	R	R'
1	Poly(methyl methacrylate)	PMMA	CH_3	CH_3
2	Poly(ethyl acrylate)	PEA	H	CH_2CH_3
3	Poly(ethyl methacrylate)	PEMA	CH_3	CH_2CH_3
4	Poly(methyl d_3-methacrylate)	d_3-PMMA	CD_3	CH_3
5	Poly(fluorooctyl methacrylate)	PFOMA	CH_3	$CH_2(CF_2)_6CF_3$
6	Poly(ethyl cyanoacrylate)	PECA	CN	CH_2CH_3

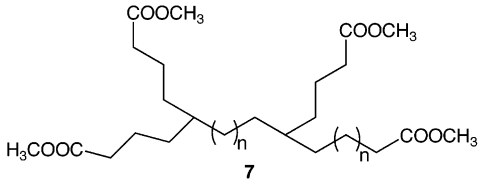

7

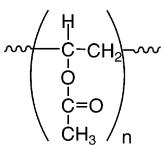

8

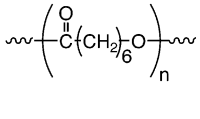

9

* To whom correspondence should be addressed. E-mail: mdef@unc.edu.

10.1021/ma047857r CCC: $30.25
Published on Web 03/22/2005

Scheme 1

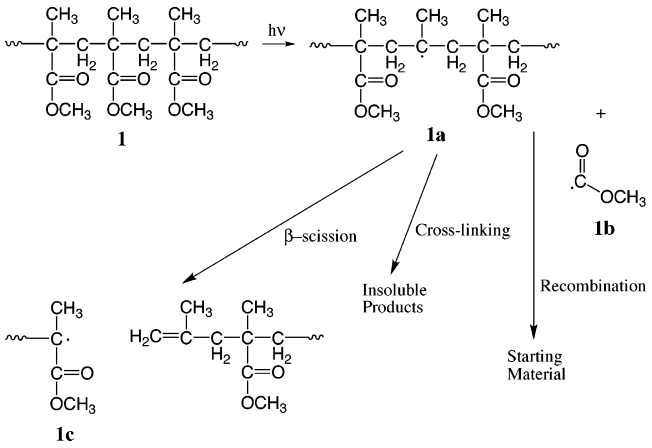

Polymer **7** has an unusual structure; it is a branched polyethylene with about 10% methyl methacrylate incorporation.[2,3] The ester functionalities in this polymer are present at the end of the branches of the polymer and not on the main polymer chain. This polymer is of interest in investigating the effect of proximity of the ester chromophores in the photodegradation process. Nonacrylic polymers **8**, poly(vinyl acetate) (PVA), and **9**, poly(caprolactone) (PCL), were also studied to see whether other ester functionalities are as photolabile as acrylic structures at 248 nm.

Propylene carbonate is the most commonly used solvent in our laboratory for TREPR experiments on nonfluorinated acrylic polymers. It is an excellent solvent for such polymers at room temperature and above. It boils at 240 °C, which allows access to high-temperature spectra even with recirculating samples, and it shows no TREPR signal when run as a blank under irradiation at 248 nm. To obtain the high-temperature TREPR spectrum of PFOMA, a solvent mixture consisting of different fluorinated hydrocarbons (FC-70, 3M Corp.) was used. This solvent system has a boiling point of 201 °C, dissolves PFOMA easily, and is also transparent at 248 nm.

The proposed mechanism for the photochemical degradation of acrylic polymers, as shown in Scheme 1 for PMMA, has been studied by steady-state EPR spectroscopy (SSEPR) for more than 50 years.[4–6] However, it was not until TREPR was applied to the problem that main chain acrylic radicals such as **1a** and the corresponding oxo-acyl counter-radicals **1b** could be observed directly and characterized. The reason for this is that β-scission of the main chain radical is sufficiently rapid that a large concentration of the so-called propagating radical **1c** builds up; therefore, this is the intermediate most often detected in SSEPR experiments. The time response of the X-band TREPR apparatus used in our laboratory is about 3 orders of magnitude faster than for the conventional SSEPR experiment (50 ns vs 40 μs). For this reason we can easily detect radical **1a** in the first few microseconds after its creation.

In our previous work we photolyzed polymer solutions with a pulsed 248 nm excimer laser, and intense TREPR signals were obtained.[1] However, because of the high degree of substitution on these polymers, especially the methacrylates, the spectra were very broad at room temperature and difficult to simulate. Alternating line widths indicative of hyperfine modulation were observed in nearly all cases near room temperature. By heating the samples in a variable temperature flow system, the

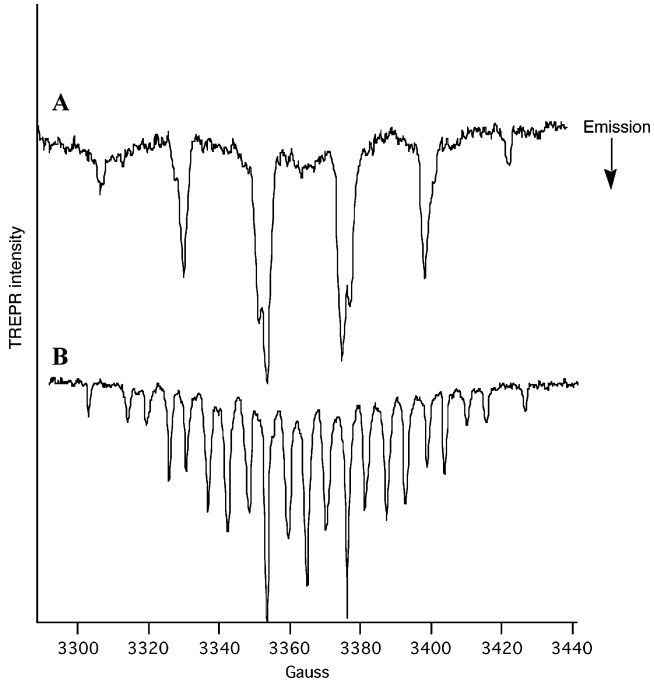

Figure 1. TREPR spectra of (A) polymeric main chain radical from PEA in propylene carbonate at 125 °C. Delay time is 0.9 μs. (B) polymeric main chain radical from PMMA in propylene carbonate at 94 °C. Delay time is 0.8 μs. The TREPR intensity (arbitrary units) and magnetic field axis shown here are the same for all spectra and are omitted in the remaining figures. In this and all subsequent spectra, lines below the baseline are in emission while those above the baseline are in enhanced absorption. Intensities of all spectra are normalized.

EPR transitions of the polymeric radicals underwent motional narrowing to give a spectrum defined by an average set of coupling constants. The observation of motionally narrowed spectra led immediately to precise simulations and therefore to high-resolution structural characterization of these intermediates for the first time.

Because of the simplicity of the fast-motion TREPR spectra, we have continued to perform our experiments at high temperatures whenever possible. In other forthcoming publications in this series we will address other issues such as the analysis of these spectra in regard to polymer chain stiffness and the transition from slow- to fast-motion EPR spectra as the temperature is raised. The goals of the work presented here are (1) to establish the generality of the proposed photochemical degradation mechanism, (2) to investigate the overall applicability of this spectroscopic technique to other polymer degradation mechanisms, (3) to investigate the onset temperature for fast motion for different acrylic main chain radicals, and (4) to unambiguously determine the structure of several polymeric main chain radicals at fast motion as a function of both main chain (α) and side chain (β) substitution.

Results and Discussion

A. General Features of TREPR Spectra of Acrylic Radicals: PMMA (1) and PEA (2). It is instructive to review the general features of main chain acrylic radical TREPR spectra at high temperatures. Figure 1 shows spectra obtained from photolysis of PEA and highly isotactic PMMA in propylene carbonate solution above 90 °C. (Except for the PMMA sample, all polymers used in this study are atactic materials.) Simulations

and characterization data for these radicals (**1a** and **2a** in accordance with Chart 1 and Scheme 1) are given in ref 1. Nuclei on the α-substituent (main chain) have hyperfine interactions with the radical center, whereas those on the β-substituent (side chain) do not. It is immediately evident from Figure 1 that α-substituents have a large effect on the appearance of the TREPR spectrum. For example, the spectrum of the radical from PEA is a well-resolved 10-line spectrum. However, the presence of a methyl group in the α-position of PMMA results in the appearance of many more lines (21 total) in the spectrum. In both radicals the β-methylene protons are diastereotopic and therefore show a splitting pattern of a triplet of triplets. In the PMMA radical spectrum there are accidental degeneracies which lead to a smaller number of observable transitions than the maximum expected ($4 \times 3 \times 3 = 36$). Analysis of the fast-motion hyperfine interactions as a function of pseudo-symmetry and stereochemistry is explained in detail in the first paper of this series.

The spectra in Figure 1 show strong net emission from the triplet mechanism (TM) of chemically induced electron spin polarization (CIDEP).[7−9] It is revealing that the dominant polarization mechanism is the TM and not the radical pair mechanism (RPM)[10,11] or spin correlated radical pair mechanism (SCRP).[12,13] The magnitudes of both SCRP and RPM polarization patterns depend on the rate of encounters taking between the two radical centers. If the mechanism of degradation of acrylic polymers is correct as shown in Scheme 1, we are creating two species, polymeric radical **1a** and oxo-acyl radical **1b**, which have drastically different diffusional properties in solution. Radical **1b** is small and will undergo much more rapid diffusion than **1a**. An immediate consequence of this is that RPM and SCRP polarization mechanisms will be quenched by relatively slow reencounter rates and can therefore be obscured in this case by the very strong TM. In all TREPR spectra detected here, emissive TM is always observed, which is unusual for aliphatic carbonyl compounds, although not unprecedented for esters.[14] We note here that in all spectra of polymeric radicals reported in this paper the TREPR transitions are emissive and therefore are recorded as transitions pointing below the baseline.

There are some other important points to be made regarding the relative intensities of the observed spin polarization mechanisms. In our previous papers it was pointed out that the β-hyperfine interactions are conformationally modulated. This can be an additional means by which the RPM polarization pattern is quenched. To understand this qualitatively, the modulation process can be thought of as a relaxation mechanism that exchanges magnetization between different nuclear spin orientations or hyperfine lines. Since these different orientations can have opposite polarizations from the RPM, the exchange of emissive and absorptive polarization cancels the intensity of the transitions in question. This is a very interesting topic in its own right and will be the subject of further quantitative study.

It is also of interest to consider why the TM polarization is so strong. We know it must be of very high magnitude because the absorbance of the polymers is quite low at 248 nm (this wavelength is just barely inside the lowest energy electronic transition, presumably n−π^*, for the ester moiety), and the quantum yield for α-cleavage is also quite small (~0.05).[15] It is well understood from CIDEP theories that slow rotational correlation times of a photoexcited state will lead to more selective intersystem crossing at the X-band field (3380 G), and this will lead to larger TM polarization. This strongly suggests that rotational motion of the ester functional group in these polymers may be quite restricted in at least one direction.

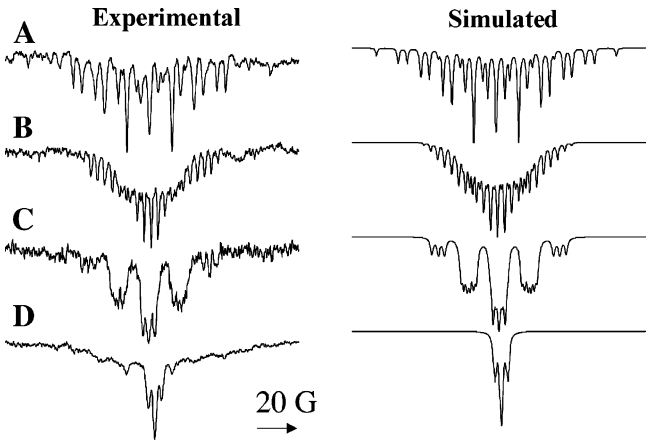

Figure 2. (Left) experimental and (right) simulated high-temperature (fast-motion) TREPR spectra of acrylic polymeric main chain radicals form the following polymers: (A) PEMA at 120 °C and delay time of 0.8 μs; (B) d_3-PMMA at 120 °C and delay time of 0.6 μs; (C) PECA at 120 °C and delay time of 0.3 μs; (D) PFOMA at 110 °C and delay time of 0.3 μs. Simulation parameters are listed in Table 1, and polymer structures are shown in Chart 1.

An oxo-acyl radical similar in structure to radical **1b** is also formed upon photolysis of PEA (it has an ethyl rather than a methyl alkyl group). However, transitions representative of this radical were not observed in our experiments. Radicals such as **1b** are expected to exhibit a single emissive peak slightly to the right of the center of the spectrum (its g-factor is slightly lower than that of the polymeric radical). The g-factor of most carbon-centered alkyl radicals is around 2.0026.[16−19] Literature values for the g-factors of oxo-acyl radicals are approximately 2.0009.[20−23] Oxo-acyl radicals have two unimolecular decomposition pathways available: loss of CO and loss of CO_2. Previous studies on the photoablation of PMMA using high-resolution MS has detected both gaseous products.[24] Griller and Roberts have determined the decarboxylation rate of an oxo-acyl radical of similar structure to be 2.1×10^6 s^{-1} at 373 K.[25] This corresponds to a decomposition time of 500 ns, which is well within the resolution time of our instrument, but the radical was not observed at any delay time from 0.1 to 10 μs.

The most likely reason for the absence of an oxo-acyl signal in the spectra from Figure 1 is fast spin relaxation. Paul has shown by line shape analysis that relaxation of an acyl radical (RC$^{\bullet}$=O) is on the order of 10 ns or faster in solution,[26] and this has recently been confirmed by the kinetic analysis acyl−alkyl biradicals by Tsentalovich et al.[27] The mechanism of this relaxation is through spin-rotational interaction in the radical, which in this case is equal to the longitudinal relaxation time T_1. Electron spin relaxation is much slower due to the hindered rotation of the polymeric radical, and therefore radical **1a** and its analogues remain spin polarized long enough to be observed by TREPR.

B. TREPR of Polymers 3−6. The TREPR spectra obtained after 248 nm photolyis of these four polymers are shown on the left side of Figure 2, along with

Table 1. Hyperfine Couplings (in G) Used in the Simulations in Figure 2[a]

polymer precursor	$\delta\ a_H(CH_3)$	$\delta\ a_H(CH_2)$	$\delta\ a_H(CH_2)$
PMMA	22.9	16.7	11.2
PEMA	22.9	15.8	11.2
d_3-PMMA	3.5	16.3	10.9
PECA	3.3 (N)	16.3	14.8

[a] PFOMA; $a_F(CF_2) = 3.2$ G, $a_F(CF_2) = 0.8$ G. All polymers above lead to main chain radicals of type **a** in Scheme 1, while PFOMA leads to radicals of type **b**.

simulations on the right side computed using magnetic parameters listed in Table 1. In Figure 2A, a TREPR spectrum is shown for the main chain radical from photolysis of PEMA, **3a**. The spectrum no longer consists of 21 lines as in Figure 1B for PMMA. Some of the previously described accidental degeneracies have been lifted to give a total of 27 lines, and the total spectral width has decreased slightly. The new lines are assumed to arise from the main chain radical and not a new signal carrier because their kinetics are identical to all the other lines and their intensity ratios are constant with temperature. These differences in hyperfine coupling constants are somewhat unexpected because the only structural difference between these radicals is the identity of the β-substituent in which the ester R group changes from methyl to ethyl.

To simulate the spectrum in Figure 2A, a hyperfine coupling constant of 22.9 G was used for the protons on the α-methyl group. Values of 15.8 and 11.2 G were used for the two sets of diastereotopic β-methylene protons. Table 1 shows how these values compare with those used for the PMMA radical **1a**. As expected, the hyperfine values for the α-methyl protons remain the same for both methacrylate polymers. The methyl group has free rotation about the C−C bond from the backbone to the methyl group, even at temperatures as low as −100 °C.[28] The additional splittings in the TREPR spectrum of radical **6a** can be simulated by changing the hyperfine values for one set of the β-methylene protons (the largest coupling constant). The value used for the radical from PEMA is approximately 1 G smaller than that from PMMA. This suggests that adding an additional methylene group to the ester group changes the relative energies of the conformations of the polymer near the radical center, which in turn affects the dihedral angles and therefore the hyperfine values. This will be discussed in more detail below.

Figure 2B shows the experimental and simulated TREPR spectra from the photolysis of d_3-PMMA (**4**) in propylene carbonate at 120 °C. The spectrum is much more narrow, and there are many more transitions than in its protonated analogue. There are many overlapping lines, and only the outermost lines of the spectrum are clearly resolved. In Table 1, it is seen that the value of the hyperfine coupling constant for the α-methyl protons has decreased from 22.9 to 3.5 G, exactly as expected for this isotopic substitution.[29] The values for the β-methylene protons used in the simulation are 16.3 and 10.9 G, which are close to the values used in the simulations of the nondeuterated polymer. The fact that they are slightly different suggests that deuteration of the polymer backbone also has an effect on the conformational energies of this polymer in solution.

Figure 2C shows the experimental high-temperature TREPR spectrum obtained during photolysis of PECA (**6**) in propylene carbonate solution, along with a computer simulation. There are five packets of lines

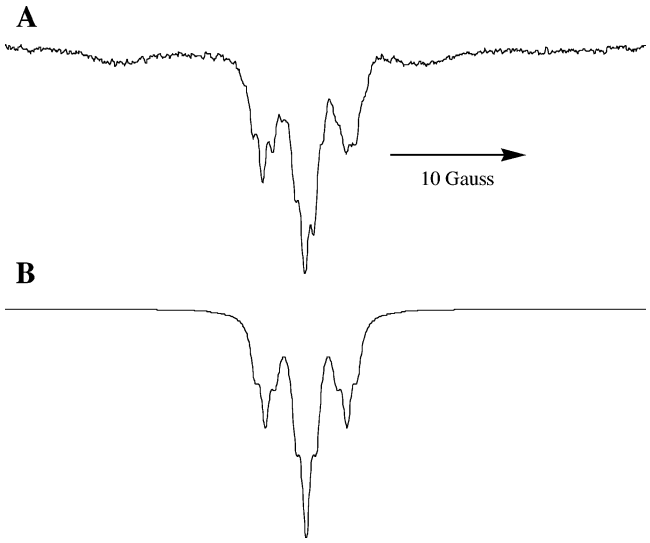

Figure 3. Experimental (top) and simulated (bottom) TREPR spectra of the oxo-acyl radical from PFOMA in the perfluorinated solvent FC-70. Sweep width is 50 G. Simulation parameters: $a_F(\gamma\text{-}CF_2) = 3.2$ G, $a_F(\delta\text{-}CF_2) = 0.8$ G, LW = 0.8 G.

from coupling to the β-methylene protons. Each of these packets of lines is split into an additional three lines from the γ-nitrogen ($I = 1$) in the nitrile group. The larger width of the second and fourth packet of lines can be explained by the diastereotopicity of the β-methylene protons. The hyperfine values used in the simulation are 3.3 G for the γ-nitrogen and 16.3 and 14.8 G for the β-methylene protons (Table 1). The difference between the hyperfine coupling constants for each of the β-methylene protons is much smaller for this polymer than for the other acrylic polymers.

An interesting feature of Figure 2C is the line width of the transitions. Line widths of 1−2 G are common in TREPR spectra of small molecules at room temperature. Small molecules have shorter rotational correlation times than larger molecules. As the motion of a molecule is restricted, either by cooling or by adding bulk, the line width in the TREPR spectrum begins to increase due to faster relaxation. If the line shape is Lorentzian, then $1/T_2 = 0.5 \times \sqrt{3} \times$ fwhm (full width at half-maximum). The line width in the simulations of Figures 1 and 2A,B does not exceed 1 G, but the line width needed to simulate the TREPR spectrum of **6a** was almost twice that value (1.8 G). This indicates qualitatively that the polymer may have a stiffer backbone than the other polymers studied here.

Figure 2D shows the experimental TREPR spectrum of the radicals from the photolysis of PFOMA (**5**). In this experiment, propylene carbonate was not used as the solvent, as it does not dissolve fluorinated polymers very well. A solvent consisting of a mixture of fluorinated hydrocarbons (FC-70, a gift from the 3M Corp.) was used. The spectrum of the polymeric radical is broad and somewhat featureless compared to other methacrylate radicals. The signal from the fluorinated oxo-acyl radical **5b** dominates the spectrum; however, it is not a singlet as observed for its protonated analogue at lower temperatures. Instead, the signal is a broad intense triplet. Upon expansion of the spectrum to a sweep width of 50 G, it can be seen that the signal is actually a triplet of triplets (Figure 3A). A simulation of this spectrum is shown in Figure 3B. For this simulation fluorine hyperfine couplings of 3.2 and 0.8 G were used.

Table 2. GPC Values Determined for Polymers before and after Photolysis[a]

	before photolysis		after photolysis	
polymer	MW	PDI	MW	PDI
a-PMMA	52K	1.53	19K	1.96
a-PMMA[b]	52K	1.53	34K	2.01
s-PMMA	7K	1.16	5K	1.27
d_3-PMMA	266K	3.89	33K	1.29
PEMA	144K	2.15	32K	1.62
PCN	22K	3.73	4K	1.26
PVA	93K	3.01	50K	3.62
PCL	41K	1.76	47K	1.55
PCL[c]	41K	1.76	47K	1.59

[a] All polymers photolyzed at 248 nm unless otherwise noted. [b] Polymer photolyzed at 193 nm. [c] Polymer photolyzed at 308 nm.

Krusic and co-workers have shown that γ- and even δ-hyperfine couplings from fluorinated radicals can be observed in SSEPR spectra due to spin polarization through C−F bonds. The coupling constants for long range fluorine hyperfine interactions are typically small, from 0.1 to 2.5 G. Our values agree well with the values of 2.6 and 0.1 G reported by Krusic et al. for γ- and δ-hyperfine ^{19}F couplings in perfluoralkyl radicals.[30−32]

In all of the spectra reported above, the polymeric main chain radical generally exhibits a very intense signal, and the oxo-acyl signal is weak or absent from the TREPR spectrum at high temperatures. The opposite relative intensities are observed for PFOMA photolysis. Oxo-acyl radical **5b** is superimposed on a large, broad signal which has some similar features to the signal from the polymeric radical of PMMA at lower temperatures (spectrum not shown). The signal carrier is most likely the main chain polymeric radical from PFOMA. The polarization from radical **5b** is much stronger than that from the polymeric radical for two reasons: One is that the same magnitude of polarization is carried by fewer spectral lines. But it is also highly likely that the fluorinated oxo-acyl radical **5b** is bulkier and more rigid than its alkyl analogues and therefore will have a much longer rotational correlation time, leading to longer spin relaxation times at X-band. This will be discussed in more detail in a subsequent paper in this series.

Polymers **7**−**9** failed to show any TREPR signals at any accessible temperature. For branched polymer **7**, it is possible that degradation is occurring, but the amount of MMA incorporation is very low in this structure so there may only be a small amount of radicals being produced. The experiment may not be sensitive enough to detect them. Poly(vinyl acetate) (**8**) has been studied previously by SSEPR and did show a signal in those experiments, so our negative result is somewhat surprising. It is possible that the radicals produced are not spin polarized to any great extent (weak TM), or they are formed in very low concentrations because the quantum yield of radical formation is low. At lower temperatures (77 K) both methyl radicals and the polymeric radical from side chain cleavage of PVA have been observed.[33,34]

No TREPR signal was observed on photolysis of PCL (**9**). From the literature on poly(esters) it is believed that the degradation mechanism for this polymer proceeds via one or more radical intermediates,[35−37] so this result is also somewhat surprising. However, as a percentage of the total molecular weight, the ester chromophores are present to a much higher degree in acrylic structures than in polymer **9**, so the lack of signals may simply be due to a low concentration of chromophore. Alternatively, the symmetry of the chromophore's triplet state and/or its rotational correlation time may not be in favor of strong TM polarization generation.

C. GPC Results. Table 2 shows typical results for the GPC analysis of some acrylate polymers before and after photolysis, which were typically run with concentrations of 15 mg/mL against a polystyrene standard. Photolysis at 248 nm results in a large reduction of the molecular weight of the polymer, as in the case of d_3-PMMA, shown in entry 4 in Table 2. Polymers that are initially fairly monodisperse (polydispersity index (PDI) < 2) show an increase in PDI. Those with broad polydispersities (PDI > 2) show a decrease after photolysis. These results are in accordance with accepted models for chain scission processes.[38] The only exception in our data is the PCL sample (**9**), which because of its additional failure to give a TREPR signal, we cannot comment on further.

Entries 1−3 in Table 2 show GPC results for PMMA photolyzed at two different wavelengths: 248 nm, where strong a TREPR signal is observed, and 193 nm, where there was no TREPR signal. In both cases, the molecular weight of the polymer decreases upon photolysis. This is strong evidence that main chain scission is occurring upon photolysis at both wavelengths. It cannot be stated that irradiation at 248 nm causes more chain cleavage simply because the drop in molecular weight is greater. The GPC samples for each of the polymers were prepared after different times of exposure to UV light of 248 nm. From the results in Table 2, it can be concluded that for all the polymers studied here main chain cleavage or β-scission is occurring after side chain cleavage. This is to be expected as the time scale for side chain scission is less than 100 ns from these experiments. It has been determined experimentally for PMMA that the half-life for β-scission is greater than 20 μs.[39]

Poly(vinyl acetate) (**8**), which did not show a TREPR spectrum upon photolysis, shows a large drop in molecular weight when studied by GPC analysis. This is in line with results by Buchanan and McGill.[40] They found that upon exposure to UV light from a Hg lamp for 30 min the molecular weight of this polymer decreased by half from 73K with a PDI of 1.83 to 36K with a PDI of 4.74. In our experiments, the photolysis time of the polymer in the EPR cavity was approximately the same time period. The polymer samples in Buchanan and McGill's work also decreased in molecular weight by about half but with a much larger increase in the PDI. The lack of a TREPR signal from the photolysis of PVA is therefore perplexing, as a reasonable amount of spin polarization from the TM would be expected from these structures. The degradation mechanism of this polymer is the subject of ongoing investigations.

In NMR experiments (^{1}H at 400 MHz, Varian), PMMA was photolyzed for 30−90 min in propylene carbonate at 100 °C and at room temperature, and then the photolyzed solution was distilled to collect any volatiles that might have formed. The colorless distillate was analyzed by NMR and found to contain methyl methacrylate monomer. This compound could only have arisen from depolymerization (main chain scission) of the propagating radical **1c**. To ensure that that the distillate collected was not residual monomer from the original unphotolyzed polymer sample, solid PMMA was placed under vacuum for over an hour and no visible amount of distillate was collected. Because there is no

Scheme 2

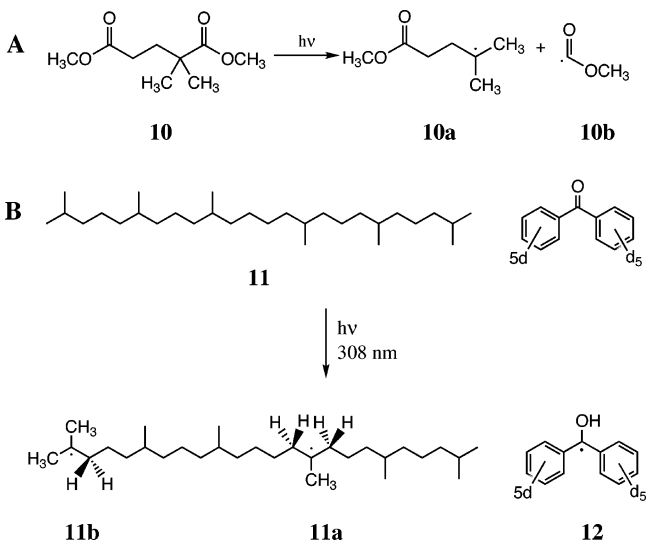

10 **10a** **10b** **11** **11b** **11a** **12**

way to produce MMA monomer other than β-scission followed by depolymerization, this further supports the mechanism shown in Scheme 1, i.e., that main chain scission is occurring during our experiments. Experimental evidence for all the steps in the mechanism in Scheme 1 has been presented.

D. Studies of Model Compounds. To further support the structural characterization of the acrylic main chain radicals, a series of model compounds were also studied by TREPR. Dimethyl-2,2-dimethyl glutamate, (Scheme 2A), is the most common small molecule used for modeling PMMA because it structurally approximates a dimer. Product analyses shows that this compound is photochemically active at 248 nm. The mechanism of decomposition proceeds through side chain cleavage of one of the ester groups.[24,41] We used the dimethylated ester instead of the tetramethylated one to control the site of side chain cleavage, for which there are two possible sites. If cleavage occurred on the left side of the diester, the resulting radical would be a less stable primary radical. This reaction produces a tertiary radical **10a** that approximates the polymeric radicals formed by photolysis of PMMA, PEMA, and others. The more probable cleavage reaction and the resulting radicals are therefore shown in Scheme 2A.

Figure 4A shows the TREPR spectrum of a 0.94 M solution of dimethyl 2,2-dimethylglutamate in methanol photolyzed at 248 nm at room temperature. This spectrum exhibits strongly emissive TM polarization similar to that observed from photolysis of the polymers presented earlier. Absent from this spectrum is the signal from the oxo-acyl radical, **10b**, again presumably due to fast spin relaxation. A simulation is shown below the experimental spectrum. Hyperfine couplings of 22.9 G for the methyl group and 17.8 G for the β-methylene group were used.

The SSEPR spectra of the diacid analogue of **10** has been measured by Fischer et al. in water and methanol solutions at room temperature.[42,43] They were able to observe the presence of the acid analogue of **10a**, the oxo-acyl radical, and an adduct due to impurities from succinic acid. To simulate the spectrum from **10a**, they used values of 23.5 G for the protons of the methyl groups and 17.5 G for the β-methylene protons. These compare favorably to the values used to simulate the polymeric radical spectra in Figure 2.

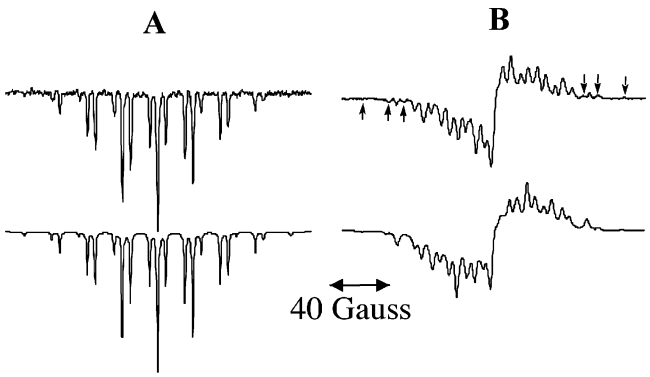

Figure 4. Experimental (top) and simulated (bottom) TREPR spectra from 248 nm excitation of small molecule model compounds: (A) dimethyl-2,2-dimethyl glutarate (0.94 M) in methanol at a time delay of 0.3 μs. Simulation parameters; $a_H(CH_3) = 23.1$ G, $a_H(CH_2) = 17.8$ G, line width = 1.0 G. (B) Benzophenone-d_{10} (0.5 M) in neat squalane at a delay time of 0.8 μs. Simulation parameters: Radical **11a**: $a_H(CH_3) = 22.9$ G, $2a_H(CH_2) = 16.9$ G, $2a_H(CH_2) = 11.8$ G, line width = 3 G. Radical **11b**: $6a_H(CH_3) = 22.9$ G, $2a_H(CH_2) = 17.5$ G. Radical **12**: $a_H(COH) = 2.2$ G, line width = 3 G. Intensity ratio of radical **11a** to radical **11b** to radical **12** is 4/2/3. Substrates and radical structures are shown in Scheme 2. Transitions due to radical **11b** are indicated by arrows.

The second model system explored was a solution of benzophenone-d_{10} in pure squalane **11** (Scheme 2B). The viscosity of the squalane solution is similar to that of the polymer solutions at room temperature. The photoexcited triplet state of benzophenone will abstract hydrogen from squalane. There are several possible abstraction sites on the squalane chain. The excited benzophenone will abstract preferentially from the those sites leading to tertiary alkyl radicals. There are two types of tertiary radical possible. The first is an internal structure, **11a**, and the other is a terminal radical, **11b** (Scheme 2B). The major difference in the two radicals is the total number of hyperfine couplings. The terminal radical (**11b**) will have eight hyperfine couplings, while the internal radical (**11a**) will only have seven. To a first approximation, radical **11a** is identical to those formed by photolysis of PMMA. In this case, the radical has a α-methyl group and two β-methylene groups. The counter-radical formed is a deuterated hydroxydiphenylmethyl radical, which gives a broad singlet in the center of the TREPR spectrum.

Figure 4B shows the experimental TREPR spectrum when deuterated benzophenone is photolyzed in the presence of squalane. The most obvious difference between the TREPR spectra of PMMA and this model compound is the different CIDEP polarization, which is predominantly from the radical pair mechanism. The RPM polarization is strong when the two radicals undergo several diffusive encounters, which is expected here due to the increased viscosity of the solutions. A simulation of the experimental TREPR data in Figure 4B is shown below the experimental spectrum. From the relative intensity of the emissive and absorptive lines, both the TM and RPM polarization mechanisms are concluded to be active. About 30% TM polarization was added into the simulations. From the wide sweep width of the outermost lines, it can be concluded that a very small amount of the terminal tertiary radical **11b** is being produced, as indicated by arrows in Figure 4B. Both tertiary radicals produced by hydrogen abstraction from squalane were included in this simulation. The hyperfine couplings used for the internal radical **11a**

are 22.9 G for the three β-protons of the methyl group and 16.9 and 11.8 G for the two sets of methylene protons. For the terminal radical **11b**, coupling constants of 22.9 G for the methyl group and 17.5 G for the β-methylene protons were used. The counter-radical **12**, a protonated benzophenone ketyl radical, was simulated as single peak with *g*-factor of 2.0032 and a line width of 3 G. The positions of the transitions are accurately reproduced; however, the individual intensities are not. This is especially true of the most central lines in the spectra, which is a common problem in CIDEP simulation routines. Despite this limitation, we can use the line positions to estimate the hyperfine coupling constants in this radical to a high degree of certainty.

The hyperfine coupling constants used in the simulation of the squalane model compound are extremely close to those used to simulate the high-temperature TREPR data of the radical from PMMA listed in Table 1 and used to generate the simulations in Figure 2 (16.7 and 11.2 G). These additional data further support the assignment. In an upcoming paper we will use these data to test the temperature dependence of the squalane-derived radicals to see whether this can be used to model the polymer chain dynamics in solution. The slight differences between the squalane radical hyperfine coupign constants and the polymer values are most likely due to slight differences in averaging at fast motion because of chain length differences.

Some additional comments should be made regarding the squalane experiments. First, the line width is significantly broader than in the polymer experiments due to the lower temperature. This is most likely just a viscosity effect on T_2. But there exists a very interesting symmetry issue in this molecule with respect to radical structure. The ground state squalane molecule has four stereogenic centers but is optically inactive due to point symmetry about the center of the $C_{11}-C_{12}$ bond (i.e., it is a *meso* compound). Since the creation of free radical centers at any carbon atom along the chain disrupts this symmetry relationship, we might expect similar diastereotopicity issues in squalane radicals as observed in our polymeric structures. Therefore, it will be very interesting to see whether higher temperature spectra lead to additional splittings as in Figure 1A for PEA. This problem, and the physical modeling of it, are outside the scope of the present paper and will not be considered further at present.

A second feature of the squalane spectrum is that the predominant spin polarization mechanism is RPM rather than TM. The TM dominates the TREPR spectra of polymers **1**−**6** as well as that from model compound **10**. The major difference for squalane is of course the method of free radical production, which takes place by H atom abstraction rather than α-bond cleavage. The typical triplet state lifetime for benzophenone in alkane solutions is about 300 ns,[44] whereas bond cleavage is nominally an order of magnitude or more faster. Since spin relaxation in the triplet state is competitive with bond cleavage, strong TM polarization is observed. This spin polarization mechanism is expected to be very weak in the squalane system due to the slow rate of reaction to produce radicals. It is interesting to note that while the RPM polarization is strong here due to the high viscosity, it may well be quenched by conformational modulation as discussed above. This is further motivation to extend our future work to the temperature dependence of the TREPR spectrum from photolysis of the benzophenone/squalane system.

Conclusions

The simulations of the high-temperature TREPR spectra presented here, coupled with the symmetry relationships given in our previous paper, lead to an unambiguous identification of the radicals produced from the primary photochemical events of acrylic polymer degradation under direct UV irradiation at 248 nm. The excellent fit of the simulations allows for assignment of the spectra with a high degree of confidence. Results from small molecule model compounds strongly support the assignments. As expected, the spectra are strongly influenced by substitution on the main chain of the polymer. A surprisingly fine sensitivity to the ester side chain structure was observed, with hyperfine couplings changing even when the β-substituent is changed from methyl to ethyl. Another example of the influence of the side chain appears to be a control of the degree of chain stiffness in PFOMA, and this will be discussed further in a subsequent publication in this series.[47]

The general photochemical mechanism for degradation of acrylic polymers appears to be the same regardless of polymer or ester side chain structure. Further spectroscopic analysis has shown some evidence for all the steps in the mechanism of acrylic polymer degradation illustrated in Scheme 1. GPC analysis of the photolyzed polymers provides proof that main chain cleavage is occurring upon irradiation, even in polymers where no TREPR signal is observed. Product analysis using NMR shows evidence of monomer formation, which can only come from β-scission of the main chain polymeric radical.

Experimental Section

A. TREPR. Continuous wave TREPR experiments were performed as previously described.[48] Briefly, all experiments were performed on a JEOL USA Inc. JES-RE1X X-band EPR spectrometer equipped with a wide bandwidth preamplifier and a low-noise GaAsFET microwave amplifier. Solutions of polymer (2.5 g) in solvent (60 mL) were circulated through a flat cell (0.4 mm path length) positioned in the center of a Varian TE_{103} optical transmission cavity. The solutions were photolyzed using a Lambda Physik Compex 120 excimer laser (248 nm, KrF) running at 60 Hz with a pulse energy of 100 mJ (~20 mJ per pulse hitting the sample) and a pulse width of 17 ns. Spectra were collected in the absence of field modulation at a fixed delay time after the laser flash using a two-gate boxcar integrator (Stanford, 100 ns gates), while the external magnetic field was swept, typically over 2 or 4 min.

B. High-Temperature Flow System. For high-temperature experiments, the deoxygenated sample solution was circulated using a micropump (Micropump model 000-405) through Teflon PFA $^1/_8$ in. tubing insulated with polyurethane foam tape. From the pump, the sample tubing passed through a copper coil wrapped with heating tape (Omega, Inc.), which was controlled using a feedback circuit between a variable power temperature controller and thermocouples placed at the entrance and exit of the quartz flow cell. The sample was recirculated between the flat cell and the reservoir. Reported temperatures are the average of three measurements from the top and bottom of the flat cell and the reservoir. The maximum temperature gradient at the highest temperature was 10 °C; therefore, all temperatures are reported as ±5 °C.

C. Commercial Samples. Samples of poly(ethyl acrylate) were a gift from the Rohm and Haas Co. and were used as received. Poly(ethyl cyanoacrylate) was a gift from the Kodak Corp. and also used as received. The fluorinated solvent FC-

70 was a gift from the 3M Corp. Propylene carbonate, squalane, and atactic PMMA were purchased from Aldrich and used as received. Poly(fluorooctyl methacrylate) was generously provided by Dr. J. M. DeSimone and used as received. The ethylene−acrylate copolymer was generously provided by Dr. M. L. Brookhart and was purified by column chromatography before use.

D. Synthesis. Unless indicated below, molecular weight data for the polymers studied are listed in Table 2.

Poly(methyl d_3-methacrylate). The deuterated monomer was synthesized via the three step method of Keah and coworkers.[49] The polymer was then synthesized by radical polymerization. GPC showed $M_N = 266$K, $M_W = 1037$K, and PDI = 3.89.

Dimethyl-2,2-dimethyl Glycidate. 25.33 g (0.16 mol) of 2,2-dimethylglycidic acid was dissolved in 150 mL of methanol, and approximately 0.5 mL of concentrated sulfuric acid was added. The reaction flask was equipped with a reflux condenser and heating mantle and set to reflux. The reaction was monitored by NMR. After 48 h, the methanol was removed by rotary evaporation. The product was dissolved in diethyl ether and dried over magnesium sulfate. The ether was removed by rotary evaporation, yielding a colorless oil (29.26 g, 98.41% yield). ^{1}H NMR (200 MHz, $CDCl_3$): $\delta = 3.65$ (s, CH_3, 6H), 2.27 (m, CH_2, 2H), 1.85 (m, CH_2, 2H), 1.97 (s, CH_3, 6H).

Highly Isotactic Poly(methyl methacrylate). Highly isotactic poly(methyl methacrylate) was synthesized by the method of Zundel.[50] GPC showed $M_N = 38$K, $M_W = 88$K, and PDI = 2.31. ^{1}H NMR (200 MHz, $CDCl_3$): $\delta = 1.20$−93% isotactic (mm), 1.00−5% atactic (mr), 0.82−2% syndiotactic (rr). Total meso dyads: 96%.

Acknowledgment. We thank the Rohm and Haas Co. for polymer samples, and the National Science Foundation for their continued strong support of our program (Grant CHE-0213516). We also thank Dr. N. V. Lebedeva for assistance with the preparation of this manuscript.

References and Notes

(1) Harbron, E. J.; McCaffrey, V. P.; Ruixin, X.; Forbes, M. D. E. *J. Am. Chem. Soc.* **2000**, *122*, 9182−9188.
(2) Johnson, L. K.; Mecking, S.; Brookhart, M. *J. Am. Chem. Soc.* **1996**, *118*, 267−268.
(3) Mecking, S.; Johnson, L. K.; Wang, L.; Brookhart, M. *J. Am. Chem. Soc.* **1998**, *120*, 888−899.
(4) Schneider, E. E.; Day, M. J.; Stein, G. *Nature (London)* **1951**, *168*, 645−646.
(5) Moore, J. A.; Choi, J. O. In *Radiation Effects On Polymers*; Clough, R. L., Shalaby, S. W., Eds.; American Chemical Society: Washington, DC, 1991; Vol. 475, pp 156−192.
(6) Carswell, T. G.; Garrett, R. W.; Hill, D. J. T.; O'Donnell, J. H.; Pomery, P. J.; Winzor, C. L. In *Polymer Spectroscopy*; Fawcett, A. H., Ed.; John Wiley & Sons: Chicago, 1996; pp 253−274.
(7) Atkins, P. W.; Evans, G. T. *Chem. Phys. Lett.* **1974**, *25*, 108−110.
(8) Wasserman, E.; Snyder, L. C.; Yager, W. A. *J. Chem. Phys.* **1964**, *41*, 1763−1772.
(9) Wong, S. K.; Hutchinson, D. A.; Wan, J. K. S. *J. Chem. Phys.* **1973**, *58*, 985−989.
(10) Pedersen, J. B.; Freed, J. H. *J. Chem. Phys.* **1973**, *59*, 2869−2885.
(11) Adrian, F. J. *J. Chem. Phys.* **1971**, *54*, 3918−3923.
(12) Closs, G. L.; Forbes, M. D. E.; Norris, J. R. *J. Am. Chem. Soc.* **1987**, *91*, 3592−3599.
(13) Buckley, C. D.; Hunter, D. A.; Hore, P. J.; McLauchlan, K. A. *Chem. Phys. Lett.* **1987**, *135*, 307.
(14) Wymann, L.; Kaiser, T.; Paul, H.; Fischer, H. *Helv. Chim. Acta* **1981**, *64*, 1739.
(15) Kaiser, T.; Fischer, H. *Helv. Chim. Acta* **1979**, *62*, 1475−1484.
(16) Paul, H.; Fischer, H. *Helv. Chim. Acta* **1973**, *56*, 1575.
(17) Kochi, J. K.; Krusic, P. J.; Eaton, D. R. *J. Am. Chem. Soc.* **1969**, *91*, 1879.
(18) Ohno, A.; Kito, N.; Ohnishi, Y. *Bull. Chem. Soc. Jpn.* **1971**, *44*, 470.
(19) Chen, K. S.; Kochi, J. K. *Can. J. Chem.* **1974**, *52*, 3529.
(20) Griller, D.; Roberts, B. P. *Chem. Commun.* **1971**, 1035.
(21) Griller, D. *J. Magn. Reson.* **1972**, *6*, 402.
(22) Hefter, H.; Fischer, H. *Ber. Bunsen-Ges. Phys. Chem.* **1970**, *74*, 493.
(23) Metcalfe, A. R.; Waters, W. A. *J. Chem. Soc. B* **1967**, 340.
(24) Krajnovich, D. J. *J. Phys. Chem. A* **1997**, *101*, 2033−2039.
(25) Griller, K.; Roberts, B. P. *J. Chem. Soc., Perkin Trans. 2* **1972**, *6*, 747−751.
(26) Paul, H. *Chem. Phys. Lett.* **1975**, *32*, 472−475.
(27) Tsentalovich, Y. P.; Forbes, M. D. E.; Morozova, O. B.; Plotnikov, I. A.; McCaffrey, V. P.; Yurkovskaya, A. V. *J. Phys. Chem. A* **2002**, *106*, 7121−7129.
(28) Spevacek, J.; Schneider, B. *Adv. Colloid Interface Sci.* **1987**, *27*, 81−150.
(29) Lambert, J. B.; Shurvell, H. F.; Lightner, D. A.; Cooks, R. G. *Organic Structural Spectroscopy*; Prentice Hall: Upper Saddle Hill, NJ, 1998.
(30) Fagan, P. J.; Krusic, P. J.; McEwen, C. N.; Lazar, J.; Parker, D. H.; Herron, N.; Wasserman, E. *Science* **1993**, *262*, 404−407.
(31) Krusic, P. J.; Kochi, J. K. *J. Am. Chem. Soc.* **1968**, *90*, 7155.
(32) Krusic, P. J.; Chen, K. S.; Meakin, P.; Kochi, J. *J. Phys. Chem.* **1974**, *78*, 2036−2047.
(33) Geuskens, G.; Borsu, M.; David, C. *Eur. Polym. J.* **1972**, *8*, 883−892.
(34) Tsuji, K. *Rep. Prog. Polym. Phys. Jpn.* **1974**, *17*, 553.
(35) Bei, J.; He, W.; Hu, X.; Wang, S. *Polym. Degrad. Stab.* **2000**, *67*, 375−380.
(36) Binns, M. R.; Lukey, C. A.; Hill, D. J. T.; O'Donnell, J. H.; Pomery, P. J. *Polym. Bull.* **1992**, *27*, 421−424.
(37) Carswell-Pomerantz, T.; Hill, D. J. T.; O'Donnell, J. H.; Pomery, P. J. *Radiat. Phys. Chem.* **1995**, *45*, 737−744.
(38) Deleted in proof.
(39) Beck, G.; Lindenan, D.; Schnabel, W. *Macromolecules* **1977**, *10*, 135−138.
(40) Buchanan, K. J.; McGill, W. J. *Eur. Polym. J.* **1980**, *16*, 313−318.
(41) Kuper, S.; Modaressi, S.; Stuke, M. *J. Phys. Chem.* **1990**, *94*, 7514−7518.
(42) Kaiser, T.; Grossi, L.; Fischer, H. *Helv. Chim. Acta* **1978**, *61*, 223−233.
(43) Wymann, L.; Kaiser, T.; Paul, H.; Fischer, H. *Helv. Chim. Acta* **1981**, *64*, 1739−1751.
(44) Murov, S. L. *Handbook of Photochemistry*; M. Dekker: London, 1993.
(45) Heller, C.; McConnell, H. M. *J. Chem. Phys.* **1960**, *32*, 138.
(46) Carrington, A.; McLauchlan, A. D. *Introduction to Magnetic Resonance*; Harper & Row: New York, 1967.
(47) McCaffrey, V. P.; Harbron, E. J.; Forbes, M. D. E. *J. Phys. Chem. B*, submitted.
(48) Forbes, M. D. E. *Photochem. Photobiol.* **1997**, *65*, 73−81.
(49) Keah, H. H.; Rae, I. D.; Hawthorne, D. G. *Aust. J. Chem.* **1992**, *45*, 659−669.
(50) Zundel, T.; Teyssie, P.; Jerome, R. *Macromolecules* **1998**, *31*, 2433−2439.

MA047857R